Dimensional synthesis of three-fingered robot hands for maximal precision manipulation workspace

Júlia Borràs[1] and Aaron M. Dollar
Mechanical Engineering & Materials Science
Yale University
New Haven, USA
{julia.borrassol, aaron.dollar}@yale.edu

***Abstract*—This paper applies dimensional synthesis to explore the geometric design of dexterous three-fingered robotic hands for maximizing precision manipulation workspace, in which the hand stably moves an object with respect to the palm of the hand, with contacts only on the fingertips. We focus primarily on the tripod grasp, which is the most commonly used grasp for precision manipulation. We systematically explore the space of design parameters, with two main objectives: maximize the workspace of a fully-actuated hand and explore how underactuation modifies it. We use a mathematical framework that models the hand-plus-object system and examine how the workspace varies with changes in nine hand and object parameters such as link length and finger arrangement on the palm.**

Results show that to achieve the largest workspaces the palm radius should be approximately half of a finger length larger than the target object radius, that the distal link of the two-link fingers should be around 1-1.2 times the length of the proximal link, and that fingers should be arranged symmetrically about the palm with object contacts also symmetric. Furthermore, a proper parameter design for underactuated hand can achieve up to 50% of the workspace of a fully-actuated hand. When compared to the system parameters of existing popular hand designs, larger palms and longer distal links are needed to maximize the manipulation workspace of the studied design.

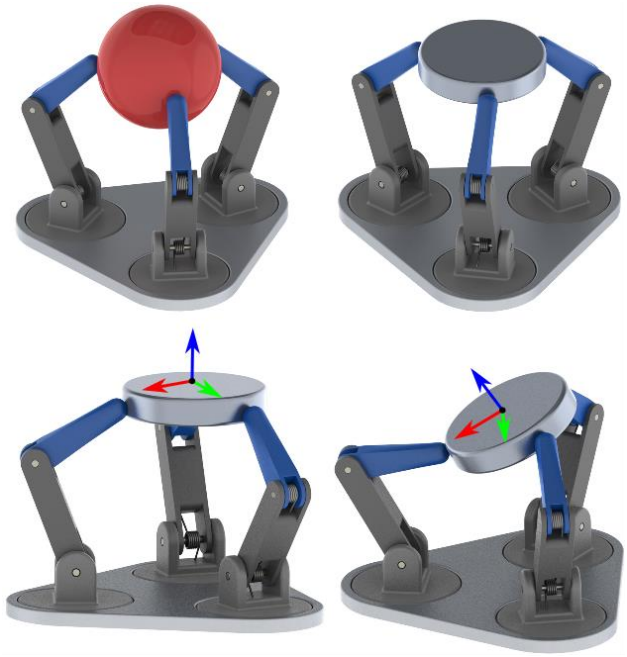

Fig. 1: Top: A simple 3-fingered hand doing two tripod precision grasps. Bottom: Two in-hand object poses. We want to explore how to optimize the geometry of the hands to maximize the number of in-hand object poses that can be achieved during in-hand manipulation without breaking contact.

I. Introduction

Robotic and prosthetic hand designers have been interested in replicating the functionality of the human hand for many decades. The human hand accomplishes both dexterous within-hand manipulation and robust grasping, but with more than 21 joints and complex tendon routing (Bullock et al., 2012b; Matsuoka et al., 2006; Grebenstein et al., 2010; Martell and Gini, 2007). Nevertheless, simpler hands with fewer joints and fingers can still achieve a high degree of functionality with a simplified structure as shown by (Mason and Salisbury, 1985; Townsend, 2000; Schunk, 2013; Salisbury and Craig, 1982; Mason et al., 2011). However, there is considerable research to be done to achieve extra functionality beyond power-grasping with simplified hands. In this paper, we examine the design of a common three-fingered arrangement, the tripod grasp (Bullock et al., 2013; Cutkosky, 1989) and Fig. 1-top, for the purposes of maximizing the workspace over which a grasped object can be repositioned in static equilibrium and without breaking contact, *i.e.* precision manipulation (Kerr and Roth, 1986; Bullock et al., 2012a) and Fig. 1-bottom. We show that smart design choices and informed parameter optimization are needed to avoid important workspace reductions.

There have been many research efforts to examine the design parameters of robotic hands and how they affect grasping performance, e.g. (Shimoga, 1996; Ciocarlie and Allen, 2011; Hammond et al., 2012; Ciocarlie et al., 2013). However, very few previous works have specifically examined the design of fingered hands for the purposes of

[1] Julia Borras Sol was at Yale University during the development of this work, but she is currently at Institute for Anthropomatics and Robotics, Karlsruhe Institute of Technology, Karlsruhe, Germany. Mail: julia.borrassol@kit.edu

large precision manipulation workspaces. Notable exceptions include the Okada Hand (Okada, 1982), Utah/MIT Hand (Jacobsen et al., 1986), with precision manipulation demonstrations by (Michelman, 1998), the Stanford/JPL Hand (Mason and Salisbury, 1985; Salisbury and Craig, 1982), the DLR Hands (Butterfaß et al., 1998; Butterfaß et al., 2001; Grebenstein et al., 2011), and the Metahand (Dai et al., 2009). However, researchers have yet to thoroughly examine how the detailed design parameters of a hand, including the finger and palm kinematics, can be synthesized in order to maximize the precision manipulation workspace of the hand grasping a range of objects held within the fingertips.

In this paper we examine the dimensional synthesis of a common class of three-fingered grasp for the purposes of investigating how variations in design parameters affect the precision manipulation capabilities, and in particular the range of positions and orientations over which a circular object held within the fingertips can be stably positioned. This class of 3-fingered grasp, with 2 links per finger, covers many popular architectures of robotic hands such as the Barrett hand (Townsend, 2000), the IPR SCHUNK Dexterous Hand SDH-2 (Schunk, 2013) and the iRobot-Harvard-Yale (iHY) Hand (Odhner et al., 2013), and it is similar to many other 3 fingered hands such as the JPL hand (Salisbury and Craig, 1982).

A second objective of the paper is to investigate how underactuated transmissions can modify the size of the manipulation workspace. Underactuated hands achieve an open-loop adaptive behavior that has proved to be very successful for power-grasping a wide variety of objects in unstructured environments (Dollar and Howe, 2010). However, such advantages come at an expense of reducing the dimension of the wrench space that can be realized at the fingertips, therefore reducing the manipulation workspace. We will quantify the reductions and show how design parameters can greatly minimize such reduction. We will also show how design parameters that lead to maximal workspaces for fully-actuated hands do not necessary lead to the maximal size for an underactuated version of the same hand.

Dimensional synthesis involves the study of the proper dimensions of a given mechanism design to improve its performance. It is well known that a manipulator with well-designed dimensions will exhibit overall better performance than one designed intuitively but with poorly chosen dimensions. However, due to the complexity of the hand structure and the high coupling between different characteristics that condition its performance, dimensional synthesis of robotic hands has not been widely applied. One of the first to apply it to robotic hands was Salisbury and Craig (Salisbury and Craig, 1982). They studied how to design fingers to avoid singularities and applied a numerical approach to define its optimal dimensions. In contrast, we will analyze the hand-plus-object and its properties as a whole using a mathematical framework from parallel manipulators adapted to robotic hands (Borràs and Dollar, 2013b; 2013a; Borràs and Dollar, 2014), using screw theory similarly as done in works like (Cui and Dai, 2012). The parallelism between parallel robots and grasping has been used before to define dexterity measures for grasping (Bicchi and Prattichizzo, 2000). In previous work we showed how two parameters related to the compliance and tendon pulling of the fingers can greatly increase the size of the manipulation workspace of an underactuated hand of a specific design (Borràs and Dollar, 2013b; Borràs and Dollar, 2014). In this work, we explore a bigger set of parameters for fully-actuated and under-actuated hands, including the geometry of the fingers, the palm and its symmetry, in combination with other parameters such as compliance and the transmission ratio that appear in underactuated hands.

This paper is organized as follows. Section II discusses the general dimensional synthesis approach taken in this paper, and Section III presents the mathematical formulation of the problem. Section IV presents the methodology for computing systematically the workspaces and calculating their size. Section V shows the results of our computations and finally Section VI discusses the results and gives some conclusions.

II. Dimensional Synthesis Approach

We proved in previous works that the hand we want to examine has the same structure as a parallel manipulator when it is holding an object with its fingertips (Borràs and Dollar, 2013a). Therefore, mathematical frameworks commonly used for parallel manipulators can be used to model the hand, adapted to include friction and contact constraints (Borràs and Dollar, 2013b; Borràs and Dollar, 2014) . As a result, both fields can benefit of mutual transfer of knowledge. In particular, in this paper we are interested in exploring dimensional synthesis results in parallel robots to be applied to robotic hands.

Indeed, the field of parallel manipulators has extensively explored dimensional synthesis. Jean-Pierre Merlet defines 4 different main approaches (Merlet, 2006a):

1. *The atlas approach*. It reduces the number of parameters to a small set and then it defines measurements for all the combinations, showing the results as a graphical representation where the optimal can be chosen visually.

2. *The cost function approach*. It defines a cost function with a weighted sum of indexes that need to be optimized, finding the design parameters that optimize it using numerical techniques.

3. *The exact synthesis approach*. It optimizes for a particular task, defined as a set of poses, velocities, and accelerations. It solves analytically the design parameters whose workspace includes the prescribed poses.

4. *The parameter space approach*. It defines a space where each dimension represents a design parameter. Each design requirement corresponds to an area of such space, and several requirement areas can be intersected. The optimal geometry search, for a solution that holds several requirements, can be done searching only in the

intersection.

The second approach is by far the most widely used in the context of parallel manipulators, but often with a single index optimization that does not take into account other requirements (Merlet, 2006a; Tsai, 1999). Defining a weighted sum of different indexes is often arbitrary and, therefore, their results can be misleading (Das and Dennis, 1997). In addition, it has already been proved in the context of parallel robots that manipulability indexes or condition numbers do not define a proper measure of quality (Merlet, 2006b), and therefore any cost function relying on those indexes can be also misleading. In conclusion, although the cost function approach could be directly applied to robotic hands, it does not seem promising because, in addition to the mentioned drawbacks, for robotic hands we need to consider additional restrictions such as contact friction constraints and fingers that can only push and not pull.

The 3rd approach becomes unwieldy when dealing with complex geometries. It has been applied for single finger design (Dai and Wang, 2007), and also for structures that take into account several fingers (Simo-Serra et al., 2012). However, it implies the resolution of very complex systems of equations and solutions are optimal only for very specific tasks that specify a discrete number of configurations and velocities in the workspace.

The 1st approach allows the exploration of the entire parameter space and therefore, it guarantees a global optimum. However, the need of presenting results graphically limits this approach to the exploration of only 2 or 3 parameters. The generalization of this concept leads to the 4th approach, where several requirements can be intersected.

For the present work, we suggest a combination of the 1st and the 4th approach. We propose a novel graphical representation of parameter spaces with more than 3 dimensions as polygons with as many vertexes as parameters. Despite the simplicity of the approach, it allows taking into account joint limits, friction cone conditions and avoidance of singularities, as the other approaches do.

As in all optimization methods, we need to establish assumptions to reduce the parameter exploration space. In our case, on the shape of the object we assume the normal to the object surface at the contact points directed towards the center of mass. That is valid for spheres, discs and other round objects, which are the most commonly grasped with tripod grasps. We also fix the structure of links and joint axis orientations. However, our results give insights to a wide range of existing hand designs and our methods could be easily applied to other designs. Finally, we focus on the maximization of the size of the workspace, not its shape or its properties. Properties like manipulability can also be included, and are analyzed in the last section of the paper.

In practice, a design process should take into consideration combined criteria including grasping and workspace. Nevertheless, this work is useful to show how optimal parameters for workspace size are significantly different from parameters for other criteria. Indeed, we show how, if the size of the workspace is ignored, particularly for underactuated hands, the resulting design could have a much reduced workspace that could greatly limit the versatility of the designed hand.

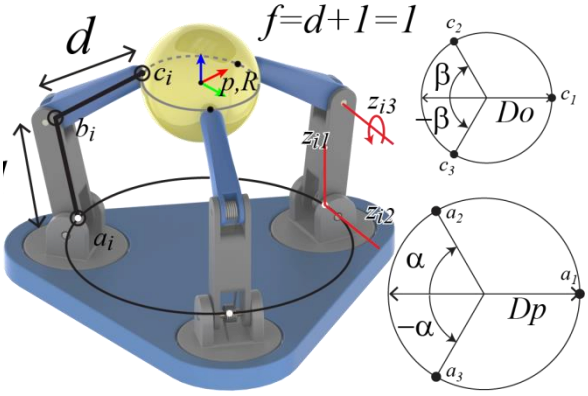

Fig. 2 Model of the studied hand (top) with its design parameters.

Table I Design parameters

Parameter	Def.	Range
P_r	D_p/f	(1,2.5)
DP_r	d/l	(0.4,2.3)
O_r	D_o/f	(0.3,1.5)
α		$(\pi/6, \pi/2)$
β		$(\pi/6, \pi/2)$
K_r	k_3/k_2	(0.5,4)
T_r	r_3/r_2	(0.6,1.2)

III. Mathematical formulation

Consider the hand-plus-object system formed by the three-fingered hand (with two-link fingers), the contact points, and the object shown in Fig. 1 and 2. Each finger i has three rotational joints with axis z_{i1}, z_{i2} and z_{i3} ($z_{i2} \parallel z_{i3}$ and $z_{i1} \perp z_{i2}$) as shown in the figure, written with respect to a fixed reference frame located at the palm, with angles of rotation θ_{i1}, θ_{i2} and θ_{i3}, respectively. The 0 angle configuration corresponds to a full opened hand with the fingers equally spread around the palm. The position and orientation of the object with respect to the palm reference frame are given by a position vector $\boldsymbol{p} \in \mathbb{R}^3$ of the center of mass (CoM) of the object and a rotation matrix $\boldsymbol{R} \in SO(3)$, together forming the object local reference frame $\{\boldsymbol{p}, \boldsymbol{R}\}$. Therfore, the object workspace is 6-dimensional. Given the object pose, if the location of the contact points in the object reference frame are given by the position vectors $\tilde{\boldsymbol{c}}_i$, we can transform them to the global reference frame as

$$\boldsymbol{c}_i = \boldsymbol{p} + \boldsymbol{R}\,\tilde{\boldsymbol{c}}_i, \qquad (1)$$

The total number of joints of the hand is $m = 9$. We represent each contact point on the object as 3 additional passive joints, acting as a spherical joint that is free to move. This is locally equivalent to the point contact with friction contact model (Borràs and Dollar, 2013a). Therefore, the total number of joints of the hand-plus-object system is $m + 9$. Let

$$\boldsymbol{q} = (\theta_{11}, .., \theta_{33})^T \quad (2)$$

be the 9-dim vector of all the hand joint angles. Any value of $\mathbf{q}$ determines a configuration of the hand, but once the object is grasped, only 6 joint angles are independent and determine the position of the object, and the rest are determined by contact constraints, namely, the fingertip contact points must remain in contact with the object at the same contact points during the in-grasp manipulation.

In our approach, we will sample the position and orientation space of the object. Each object pose determines the location of the contact points through equation (1) that are used to solve the inverse kinematics of each finger to obtain the corresponding configuration of the hand. Details on how to solve the kinematics can be found in (Borràs and Dollar, 2013b).

A. Fully actuated hand static equilibrium equations

There are several approaches to define the matrix that maps the joint velocities $\dot{\mathbf{q}}$ to the platform/object 6-dim twist $\boldsymbol{v}$ (Tsai, 1999). Here we will use the theory of reciprocal screws using the framework presented in (Borràs and Dollar, 2014), that is based on a parallel robot framework (Mohamed and Duffy, 1985). The matrix $\boldsymbol{J}$ is called the Jacobian matrix of the system, and defines the linear relationship between the object twist and the velocities at the joints as

$$\boldsymbol{J}\boldsymbol{v} = \dot{\mathbf{q}}. \quad (3)$$

It is well known that the same matrix, transposed, describes the mapping between external transmitted wrench on the object and the torques exerted at the joints. Then, if $\boldsymbol{w}$ is the total external 6-dim wrench acting on the object, and $\boldsymbol{\tau}$ is the 9-dim vector of torques exerted by each joint, we can write

$$-\boldsymbol{w} = \boldsymbol{J}^T\boldsymbol{\tau} \quad (4)$$

For the studied manipulator, the Jacobian is a 6×9 matrix expressed as $\boldsymbol{J}^T = (\cdots \boldsymbol{s}_{i1}\ \boldsymbol{s}_{i2}\ \boldsymbol{s}_{i3} \cdots)$, for $i = 1,2,3$, where each column $\boldsymbol{s}_{ij}$ is the 6-dim jth wrench of the finger i , and they are of the form

$$\boldsymbol{s}_{ij} = (\boldsymbol{g}_{ij}, \boldsymbol{h}_{ij}), \quad (5)$$

where $\boldsymbol{g}_{ij}$ corresponds to the force part of the wrench, and $\boldsymbol{h}_{ij}$ the rotational-moment part.

Equation (4) defines the static equilibrium of the hand-plus-object. From equation (4) and (5) we can rewrite the fingertip forces with respect to the palm reference frame as

$$\boldsymbol{f}_i = \sum_{j=1}^{3} \tau_{ij}\boldsymbol{g}_{ij}, \quad i = 1,2,3 \quad (6)$$

This fingertip force ignores the rotational part of the wrenches (the moment) because with the point with friction model, the moments are not transmitted to the object.

A configuration can only be considered inside the manipulation workspace if it is in static equilibrium and the corresponding fingertip forces are inside the friction cones.

To check the friction cone conditions, we need some information about the object. As we mentioned, we assume the vector normal to the plane tangent to the surface of the object at the contact normal to be directed towards the center of mass, located at $\boldsymbol{p}$. Therefore, it can be defined as $\boldsymbol{n}_i = \boldsymbol{p} - \boldsymbol{c}_i$, where $\boldsymbol{c}_i$ is the contact point. The fingertip force obtained in equation (6) is then inside the friction cone if the projection on that normal vector ${}^{n}f_i = \boldsymbol{n}_i^T\boldsymbol{f}_i$, and the projection on the normal plane to the vector, ${}^{\perp}f_i = ||\ (\boldsymbol{Id} - \boldsymbol{n}_i^T\boldsymbol{n}_i)\ \boldsymbol{f}_i\ ||$ satisfy

$${}^{\perp}f_i \leq \mu\ {}^{n}f_i, \quad (7)$$

where μ is the coefficient of friction and is taken as 0.7 for the executions.

Note that the formulation introduced so far is general and can be applied to any hand following results in (Borràs and Dollar, 2014).

B. Underactuated hand static equilibrium equations

When using underactuated fingers, there are more joints than actuators. Many of the latest underactuated hands use tendon cables combined with compliant joints (Dollar and Howe, 2010; Odhner et al., 2013) as in Fig. 3 . For these hands, we can model the transmission mechanism as a coupling between the torques exerted by the joints actuated by the same cable. Following results in (Balasubramanian et al., 2012), assuming that the tendon remains in contact with the pulley, and the pulley radii are constant, such coupling depends only on the ratio between the radii of the pulleys, which we call the transmission ratio T_r.

We consider the 2nd and 3rd joints of each finger i (with axes of rotation z_{i2} and z_{i3} in Fig. 2) to be compliant and actuated by the same pulling cable, as the two joints in the finger of Fig. 3, while the first joints of the fingers are independently actuated. As shown in Fig. 3, there is a pulling cable and torsion springs in parallel with each of the joints. Therefore, the torque exerted by each of these joints can be decomposed into the torque exerted by the cable plus the one done by the spring according to Hooke's law:

$$\tau_{ij} = {}^{a}\tau_{ij} - k_j(\theta_{ij} - \delta_j) \quad (8)$$

for each finger $i = 1, 2, 3$ and joint $j = 2, 3$, where $k_j > 0$ is the spring stiffness constant of the jth joint spring in each finger i and δ_j is its resting configuration angle. Note that $k_1 = 0$. Note that this expression can be expressed for any hand with any tendon routing configuration.

For a given configuration and a given external applied force, substituting (8) into the system in (4) leads to a linear system where the unknowns are the 9 actuation torques

$$-\boldsymbol{w} = \boldsymbol{J}^T\,{}^{a}\boldsymbol{\tau} + \boldsymbol{J}^T\,{}^{c}\boldsymbol{\tau}, \quad (9)$$

where we have split the vector of torques into the actuation torques ${}^{a}\boldsymbol{\tau} = ({}^{a}\tau_{ij})$ and the compliant torques ${}^{c}\boldsymbol{\tau} =$

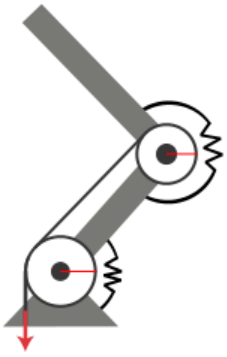

Fig. 3: Simple scheme of an underactuated finger using tendon cables that cross multiple passive compliant joints. The pulley radii are shown in red.

$(-k_j(\theta_{ij} - \delta_j))$. As the actuation torques exerted by the same cable only depend on the radius of the pulley, they are proportional, and we can write ${}^a\tau_{i3} = T_r\ {}^a\tau_{i2}$, where T_r is the ratio between the radius of the 3th joint pulley and the radius of the 2nd joint pulley. Thus, we can rewrite ${}^a\boldsymbol{\tau}$ as a 6-dimensional vector, and the above system can be rewritten as

$$-\boldsymbol{w} = \boldsymbol{J}_a^T\ {}^a\boldsymbol{\tau} + \boldsymbol{J}^T\ {}^c\boldsymbol{\tau}, \quad (10)$$

where $\boldsymbol{J}_a^T$ is a 6×6 matrix obtained from $\boldsymbol{J}^T$ combining the columns as

$$\boldsymbol{J}_a^T = (\cdots, \boldsymbol{s}_{i1}, \boldsymbol{s}_{i2} + T_r\boldsymbol{s}_{i3}, \cdots). \quad (11)$$

Note that a solution of the system would represent a valid configuration only if the cables are exerting a positive force. Depending on the routing of the cable, the tendons always exert torque of the same sign; in this case, we choose it to be positive.

In conclusion, when computing the workspace, we consider a configuration to be inside the kinematic workspace if it satisfies the following conditions:

- The position and orientation has a real inverse kinematic solution.
- The flexion finger joint angles are between 0 and 90^o.
- The angle between the vectors $\boldsymbol{c}_i - \boldsymbol{b}_i$ (following the contact phalange) and the vector normal to the object surface at the contact point is larger than 120deg. We consider this restriction because we are approximating a rolling contact with a point contact, which only holds locally, *i.e.*, close to a chosen home configuration.

If all the joints are actuated, as in a fully actuated hand, the static equilibrium equations in (4) have a 3-dimensional solution, and therefore, in a generic configuration, there is always a solution that satisfies (7), assuming that we don't limit the actuation torques values. Therefore, all the configurations in the kinematic workspace are theoretically part of the manipulation workspace of the fully actuated version of the hand.

On the contrary, for the underactuated version of the hand, only a 0-dimensional solution of the static equilibrium equations exists. Therefore, not all the configurations in the kinematic workspace will be feasible. In other words, in addition to the previous conditions, a configuration is considered to be inside the manipulation workspace of the underactuated version of the hand if

- it satisfies static equilibrium equations (10),
- the corresponding fingertip forces are inside the friction cones, and
- the actuation torques exerted by the tendon cables are positive.

To obtain the overall maximum without falling into local minima, we explore all possible configurations of the hand-plus-object according to a given 6-dim discretized space of poses for the object (Fig. 4), and for a given external applied force. If for a configuration and a force there is a solution of the static equilibrium equations that satisfy the conditions listed above, it means that the configuration belongs to the manipulation workspace of the underactuated hand. Also, we simplify further the problem considering only forces of magnitude 0. In this situation, the actuation torques are still not zero as they need to compensate for the force done by the compliant joints, and results are valid for external forces of small magnitudes in any possible direction.

Finally, we want to note that we do not study how to control the hand to move from one configuration to another. However, transitions from one point to another are possible, and could be obtained using an energy minimization problem as suggested in (Odhner and Dollar, 2011).

For the simulations in this work, we do not limit the torque the motors can exert, but we do discard singular configurations. These are configurations in which the Jacobian matrix is very close to being rank deficient, and we cannot solve the linear system in (10). In the field of parallel robots, singularities have been widely studied, for details, see (Gosselin and Angeles, 1990). For configurations closer to a singularity, the magnitude of the torques can grow infinitely and thus, in practice, the size of the manipulation workspace can be limited by this factor. However, for fully-actuated hands usually a solution can be found with minimized torques, and for underactuated hands we will see how we can reduce the exerted torques by modifying some of the stiffness constants without modifying the direction of the fingertip forces, and thus, without modifying the size of the manipulation workspace.

IV. Methodology

We distinguish two types of parameters: geometric parameters and manipulation parameters. The first group defines the geometry of the hand and they are sufficient to compute the kinematic workspace defined by just solving the kinematics. This is enough to compute the workspace of fully-actuated hands. The second group is related to compliance and transmission ratios parameters that are necessary to compute the workspace of the underactuated hand.

To normalize the results across different hand sizes we consider a fixed finger length of 1[2], and we define ratios of parameters for this fixed finger length (Fig. 2 and Table I):

- P_r Ratio between the diameter of the palm and the length of the finger
- O_r Ratio between the diameter of the object and the length of the finger
- $DP_r = d/l$ Ratio between distal (d) and proximal (l) link lenghts. Because we fix $d + l = 1$, it is equivalent to give values to the proximal link length l instead.
- α : Angle (in rad) of polar coordinates for the palm finger attachments $\boldsymbol{a}_2$ and $\boldsymbol{a}_3$ (see Fig. 2).
- β: Angle (in rad) of polar coordinaes for the contact points $\boldsymbol{c}_2$ and $\boldsymbol{c}_3$ (see Fig. 2).

The two angle parameters encode the symmetry of the hand, being symmetric with respect to all fingers when $\alpha = \beta = \pi/3$. Note that the geometrical parameters above are enough to solve the kinematics.

[2] The paper omits the units because they are not relevant for the method. By default, consider ISU: meter (m), radian (rad) and Newton (N). The results are scalable to any hand size desired.

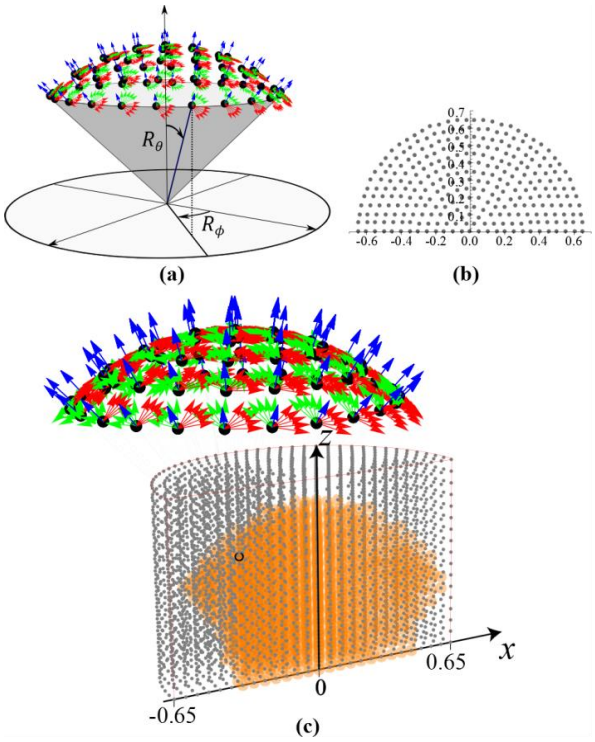

Fig. 4 **(a)** Discretization for orientations. Each red-green-blue set represents the orientation of the object reference frame, as in the two examples in Fig. 1-bottom **(b)** Discretization for positions X-Y . The ranges and intervals of discretization for position and orientations are shown in Table II. Note that the interval for R_ϕ depends on a parameter r that codifies how away you are from $R_\theta = 0$. **(c)** Combination of position and orientation discretization. For each position, we consider the set of orientations in **(a)**. We also show an example of position workspace in orange.

Table II Discretization parameters

	Range	**Interval**
x, y	$(-0.65, 0.65)$	0.05
z	$(0.2,1)$	0.05
R_z	$(-\pi/6, -\pi/6)$	$\pi/12$
R_θ	$(-\pi/4, \pi/4)$	$\pi/16$
R_ϕ	$(0, \pi)$	$\frac{2\pi}{(r+1)6}$

The manipulation parameters are

- $K_r = k_3/k_2$ Stiffness constants ratio between the 3th and the 2nd joint springs.
- k_2 Stiffness constant of 2nd joint springs
- T_r Transmission ratio, *i.e.*, ratio between the pullies radii of the 3th and 2nd joints.
- δ_2 and δ_3: resting configurations of the springs.

We are considering cables pulling in an active close mechanism, hence we set the two resting configuration angles of the springs to 0, so that the resting configuration is the hand opened. We also consider a null external force. Then, we can rewrite the static equilibrium equations (10) as

$$-k_2 \boldsymbol{J}^T \begin{pmatrix} \boldsymbol{K}_1 & 0 & 0 \\ 0 & \boldsymbol{K}_2 & 0 \\ 0 & 0 & \boldsymbol{K}_3 \end{pmatrix} \boldsymbol{q} = \boldsymbol{J}_{\boldsymbol{a}}^T \, {}^a\boldsymbol{\tau}, \qquad (12)$$

where $\boldsymbol{K}_i$ are the stiffness matrices of each finger and have the form

$$\boldsymbol{K}_i = \begin{pmatrix} 0 & 0 & 0 \\ 0 & 1 & 0 \\ 0 & 0 & K_r \end{pmatrix},$$

and $\boldsymbol{q}$ is the vector of joint angles defined in (2).

From system (12) we can state that the actuation torques ${}^a\boldsymbol{\tau}$ are proportional to k_2. In addition, form equation (6) we can write the fingertip force as

$$\begin{aligned} \boldsymbol{f}_i &= \tau_{i1}\boldsymbol{g}_{i1} + \tau_{i2}\boldsymbol{g}_{i2} + \tau_{i3}\boldsymbol{g}_{i3} = \\ &({}^a\tau_{i1}\boldsymbol{g}_{i1} + ({}^a\tau_{i2} + k_2\theta_{i2})\boldsymbol{g}_{i2} + (T_r\,{}^a\tau_{i2} + K_r k_2 \theta_{i3})\boldsymbol{g}_{i3} = \\ &{}^a\tau_{i1}\boldsymbol{g}_{i1} + {}^a\tau_{i2}(\boldsymbol{g}_{i2} + T_r\boldsymbol{g}_{i3}) + k_2(\theta_{i2}\boldsymbol{g}_{i2} + K_r\theta_{i3}\boldsymbol{g}_{i3}). \end{aligned} \qquad (13)$$

As before we concluded that the actuation torques, ${}^a\tau_{i1}$ and ${}^a\tau_{i2}$, are all proportional to k_2, the last expression in (13) is all proportional to k_2, and so, we can conclude that fingertip forces are proportional to k_2. In other words, when no external force is considered, the parameter k_2 only modifies the magnitude of the fingertip forces, but not their direction. Note that this is not true under the presence of an external force, but in our case it allows us to remove k_2 from the parameter space. Results are orientative and valid for small external forces. In addition, the value of k_2 can also be used to reduce the mangitude of the actuation torques. As we are interested in small actuation torques, we set $k_2 = 0.5$.

	Step x,z	**# Positions**	**# Orientations**	**Total # of poses**
1	0.07	1,740	111	193,140
2	0.07	1,740	305	530,700
3	0.05	4,879	111	541,569
Used	0.05	4,879	305	1,488,095
4	0.03	19,305	305	5,888,025
5	0.05	4,879	1,519	7,411,201
6	0.03	19,305	1,519	29,324,295

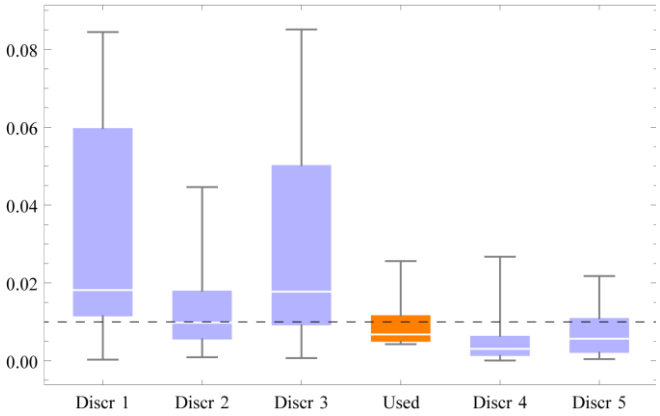

Fig. 5 Table with different workspace discretizations and the mean errors obtained when computing the size of the workspaces compared to the sizes obtained using the 6th optimization (with 29 million configurations) .

A. Discretization of the workspace

We consider a discretization of the workspace in position and orientation. Each kinematic workspace will be a subset of all the configurations and each manipulation workspace of the underactuated hand version a subset of the kinematic workspace. The chosen discretization is shown in Table II

and Fig. 4. The step in x and z is 0.05[3] and the positions are distributed radially as in Fig. 4-**(b)**. The orientations are sets of rotation matrices $\boldsymbol{R} = (\boldsymbol{i}, \boldsymbol{j}, \boldsymbol{k})$, where vectors $\boldsymbol{k}$ (in blue in the figure) represent the vector normal to the plane formed by the 3 contact points, and they are distributed around a sphere that represents the span of orientations around OX and OY (Fig. 4-**(a)**). For the discretization used, a total of 4879 positions are combined with 305 orientations at each position, leading to 1,488,095 object poses. The range of motion considered for each pose parameter is shown in the table II.

We define the size of the workspace by simply counting the number of configuraitons inside the workspace. As we are only interested in choosing the parameters with bigger workspace, we do not need to define a proper volume, but just compare between different sizes.

We are looking for the biggest workspace, and therefore we want to know if the discretization of our workspace is affecting at the order in size of different computed hand workspaces. To study this, we computed the size of the kinematic workspaces of 20 well-distributed different geometries of hands using 6 different discretizations, described in the table in Fig. 5-top. Each discretization considers increasing number of object poses, being number 6 the most accurate one with a total of more than 29 million poses.

For each discretization, we computed the size of each workspace and divided its value by the biggest one, so that for each discretization, we have a list of sizes for each 20 hands that range from 0 to 1:

$$disc_i = \{\ {}^i ws_1, \dots,\ {}^i ws_{20}\}, \qquad i = 1, \dots, 6$$

Note that in each list $disc_i$ at least one value is 1. The values obtained for the most accurate discretization, $disc_6$, were the closest to the truth, and so, we compared all the rest to them:

$$disc_i = \{\ {}^i ws_1 - {}^6 ws_1, \dots,\ {}^i ws_1 - {}^6 ws_{20}\}, i = 1, \dots, 5$$

Fig. 5-bottom shows the mean values of the above values for each discretization. In other words, the bars represent the mean differences in size for all the 20 hands. We can see that for the used discretization, the obtained erros are, at the maximum, only 0.03 (that is, the workspace sizes are 3% different than sizes computed with discretization number 6), and the mean difference is only 1% (indicated by the dashed line in the graphic). Therefore, for the results shown in the next section, we always consider as optimal the best 2% sizes.

V. Results

We considered first the full actuated hand and we swept all the geometric parameters: palm, distal-proximal ratio, and the size of the object. The length of the fingers are fixed, $l + d = 1$, therefore, the range shown for DP_r corresponds to lenghts of the proximal link from 0.3 to 0.7.

Using the discretization selected in the previous section, we checked the 1,488,095 possible configurations for each combination of geometric design parameters for the ranges shown in the Table I. The obtained 2% maximum size of the workspaces for a fully actuated hand is 124,451 and 122,914 configurations. The maximum sizes are obtained with the geometrical parameters

$$\{P_r = 1.5,\ l = 0.4\ ,\ O_r = 0.3\},\ \text{and}$$
$$\{P_r = 1.25,\ l = 0.4\ O_r = 0.3\}, \qquad (14)$$

respectively.

Table III Geometrical parameters of the 10 biggest workspaces for a fully actuated hand and the maximum underactuated hand workspace achievable.

P_r	l	O_r	F-A	K_r	T_r	U-A	%
1.25	0.3	0.3	68,178	4	1.2	19,468	28.5
1.	0.5	0.3	74,928	4	1	40,623	54.2
1.5	0.6	0.3	75,709	4	0.6	40,253	53.2
1.75	0.4	0.6	78,652	4	0.9	23,749	30.2
1.25	0.6	0.3	87,001	4	0.7	44,462	51.1
1.5	0.3	0.3	101,191	4	1.1	20,639	20.4
1.5	0.5	0.3	108,369	4	0.7	45,456	41.9
1.25	0.5	0.3	117,999	4	0.8	52,441	44.4
1.25	0.4	0.3	122,914	4	1.1	41,859	34.1
1.5	0.4	0.3	124,451	4	0.8	36,035	28.9

Fig. 6–top shows the evolution of workspace size when the geometric parameters change for different object sizes. The color bar on the left represents the evolution of the fully-actuated workspace size, from the biggest size obtained with dark color (124,451 configurations) to 0 configurations (light color). The figure shows that, when the object size increases, we can observe that palm size increases accordingly, while the optimal proximal link length slightly decreases.

We performed a similar simulation computing the size of workspaces for the underactuated hand defined in the previous section, using the sweeping of the same geometric parameters, and adding the sweeping of T_r from 0.6 to 1.2, and fixing $K_r = 4$. Fig 6– bottom shows the results following the color bar on the right from the maximum obtained size in dark color (52,441) to 0 with light color.

From Fig. 6 we can observe that the optimal trends for palm-object sizes are similar for fully and under-actuated hands. However, the sizes of the fully-actuated hand workspaces are big consistently for wide ranges of the proximal link length, while the proximal link length needs to be close to 0.5 for underactuated hands, independently of the transmission ratio used.

Table III shows the results of the 10 best fully actuated workspaces. The table contains also the maximal underactuated hand workspace that can be achieved with each corresponding geometrical parameters and the manipulation parameters needed to obtain it. The last column show the percentage of the fully-actuated hand workspace that is part of the underactuated hand workspace. We can see that using underactuation implies a reduction between 80 to 50% of the workspace. However, our computations indicate that the lost configurations are always located at the border, away from the inside/central

[3] Again, we omit units because it is all scalable according to the size of the finger. Using the ISU, that would be 0.05m for a 1m finger.

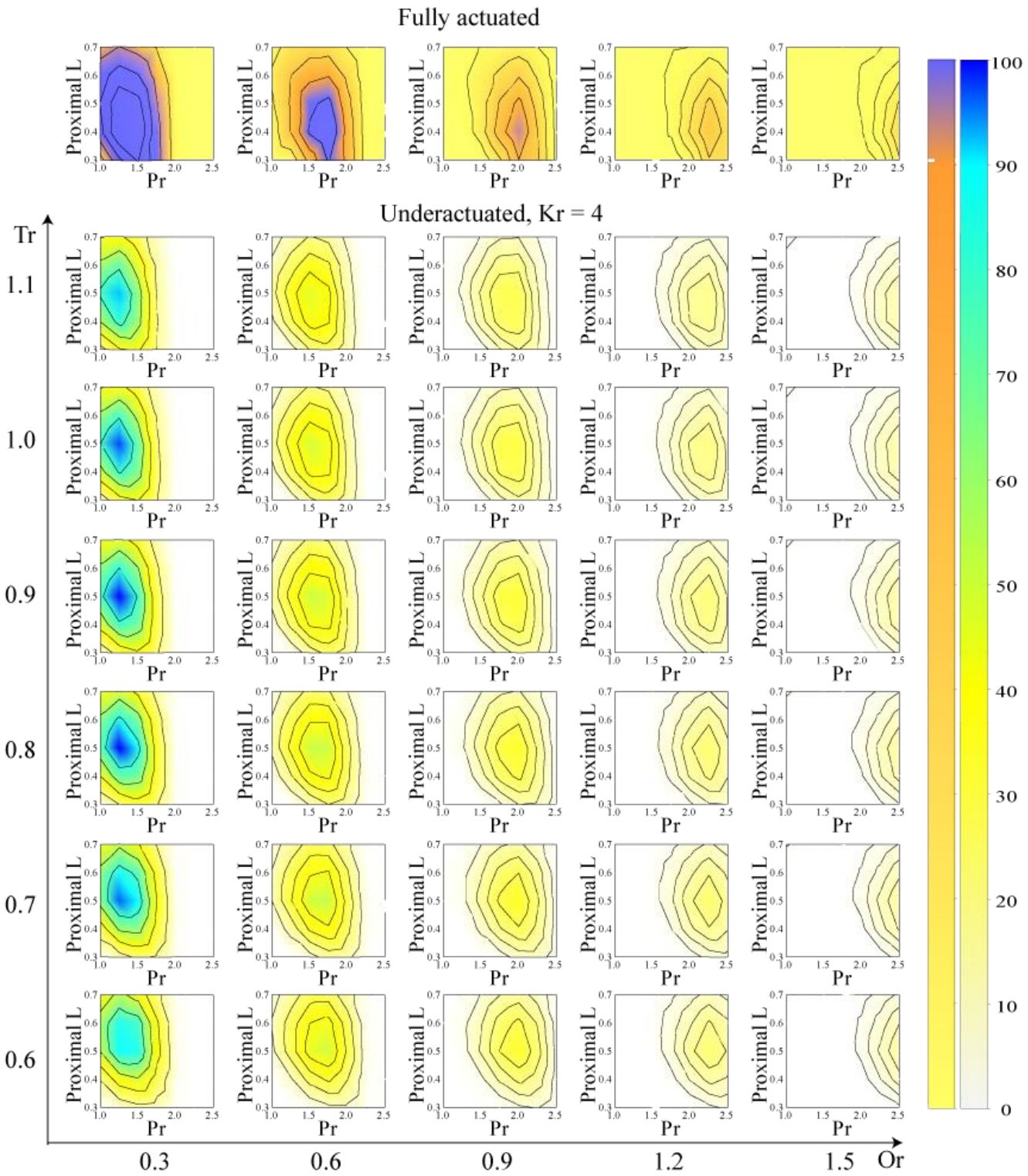

Fig. 6 Contour plots between proximal link length and palm size for growing size of the held object. The first row show results of a fully actuated hand, following the first color bar code whose maximum value is 124,451 configurations. The rest of the rows show results for the underactuated hand for the same object sizes and different values of transmission ratio from 0.6 to 1.1, following the second color bar code that reaches a maximum value in blue of 52,441 configurations.

configurations, which are in practice most likely to be part of feasible workspace when taking into account rolling contacts and motor torque limits.

Table III also tells us that the biggest size of underactauted hand workspace does not coincide with the optimal for the fully-actuated hand. Indeed, with the optimum geometric parameters ($P_r = 1.5$, $l = 0.4$, $O_r = 0.3$) the maximum feasible workspace that can be obtained with underactuation is only 36,035 configurations, with $T_r = 0.8$, but the size of the biggest underactuated

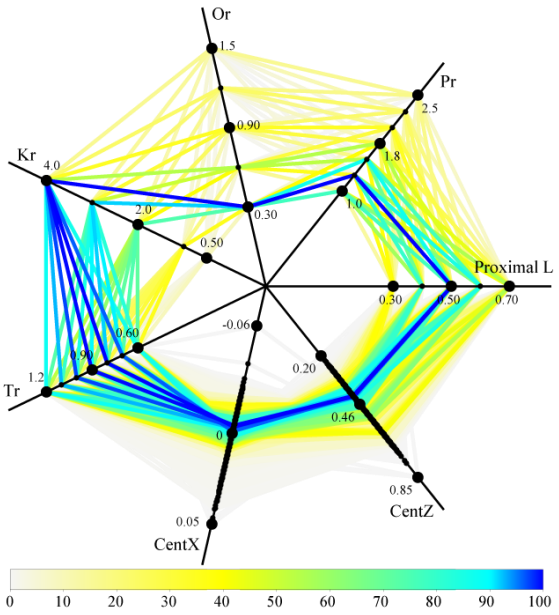

Fig. 7 Each polygon vertex lies on the axis of one of the parameters, at the length of the corresponding value of the parameter. The color of each polygon represents the size of the corresponding workspace for the underactuated version of the hand.

workspace is 45.5% bigger. This is an important result, because it shows us that for an optimal size of workspace for an underactuated hand, it is not enough to use an optimal fully actuated hand, but an independent optimization needs to be computed.

Therefore, we run an independent simulation by sweeping all the parameters in the ranges shown in the Table I, including the stiffness ratio, but fixing α and β at $\pi/3$ (for a symmetric hand with respect to each finger), to compute the sizes of the underactuated hand workspaces.

We computed a total of 6125 workspaces. The 2% maximum obtained workspaces for the underactuated hand contain 52,441 and 52,321 configurations and they are obtained with the parameters

$\{P_r = 1.25, l = 0.5, O_r = 0.3, K_r = 4, T_r = 0.8\}$ and (15)

$\{P_r = 1.25, l = 0.5, O_r = 0.3, K_r = 4, T_r = 0.9\}$, respectively.

The results are plotted in Fig. 7. To be able to plot the 5 dimensions of the parameter space, we plot a polygon for each set of data (parameters, size), where each polygon vertex corresponds to the value of the parameter and the color code represents the size of the workspace, compared to the biggest one, and thus, ranging from 0 to 100. In additon to the 5 parameters, each polygon has 2 extra vertexes that correspond to the coordinates x and z of the centroid of the computed workspace.

As the object size is not a proper hand parameter, Fig. 8 shows the same data set, plotting separetely the results for different sizes of the object, where the colors range again from 0 to 100, but they are scaled using the biggest size obtained for each object. The maximum workspace size in each plot compared to the overall maximal workspace is indicated at the top of each plot. Below each plot, we show a representation of the hand design that has the biggest workspace.

From Fig. 8 we can observe several trends. For instance, the maximum size is always obtained at the maximum stiffness ratio. We analyze in depth this relationship in section V.A. Also, the optimal size of palm and object grow proportionally, at a ratio fairly constant of $P_r - O_r \approx 1$, that is, the radii difference between palm and object is about half of the length of the finger. Section V.B will study this trend in detail.

A. On the stiffness constant

From the above simulation we observed that the biggest workspace of the underactuated hand is always obtained for the maximum stiffnes ratio possible.

To study this in detail we fixed all the parameters except the stiffness ratio, to $P_r = 1.2$, $DP_r = 1$, $O_r = 0.25, \alpha = 0.87, \beta = 1.04$ and $T_r = 0.8$. Then, we computed the size of fully-actuated hand workspace and the size of the manipulation workspace of the underactuated hand for growing values of K_r, from 4 to 70.

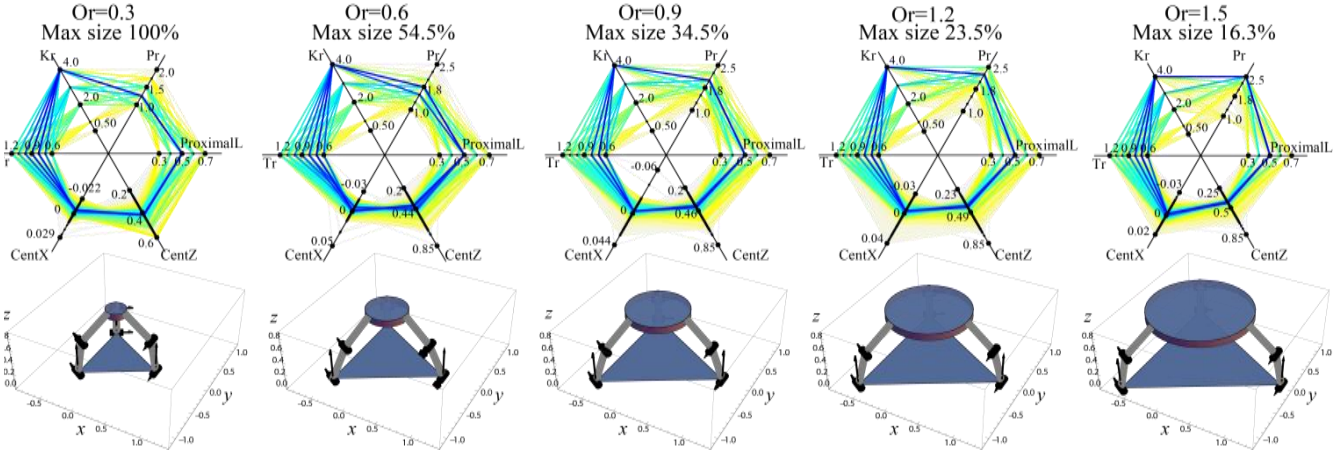

Fig. 8 The same set of data represented in Fig. 7 here is separated into different object sizes. The colors are scaled depending on the maximum size for each object size. Below each plot, a representation of the underactuated hand design using the parameters leading to bigger workspaces for each object size.

We obtained that the size of the manipulation workspaces of the underactuated hand does increase for bigger stiffness ratios, up to maximum value that, for this particular design, was close to 50% of the workspace of the fully-actuated hand. However, the magnitudes of the necessary actuation torques to obtain static equilibrium also growed.

Fig. 9 shows the relationship between the median motor torque accross the workspace with the size of the workspace for different values of stiffness ratios. It can be observed how above $K_r = 8$, the size of the manipulation workspace can only grow a maximum of 2% more, but the values of the median actuation torques grow exponentially. Therefore, we need to chose a stiffness ratio as big as possible in accordance with the limiation of the motors of our hand.

We have also analized the location of the new configurations when the stiffness ratio grows. Our results indicated that the new configurations are always at the border of the workspace. In other words, when reducing the stiffness ratio to save motor enery, we will be only losing configurations away from the centrer position. Representations of the shape of the manipulation workspace can be found in Section V.D.

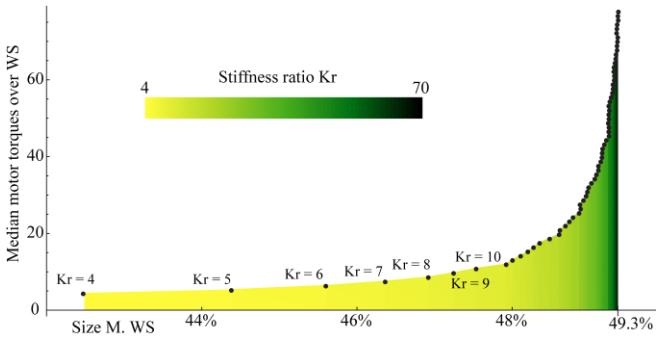

Fig. 9 Tradeoff between size of the manipulability workspace (that goes up to 49% of the kinematic workspace) versus motor torque values, that grows linearly with the value of K_r.

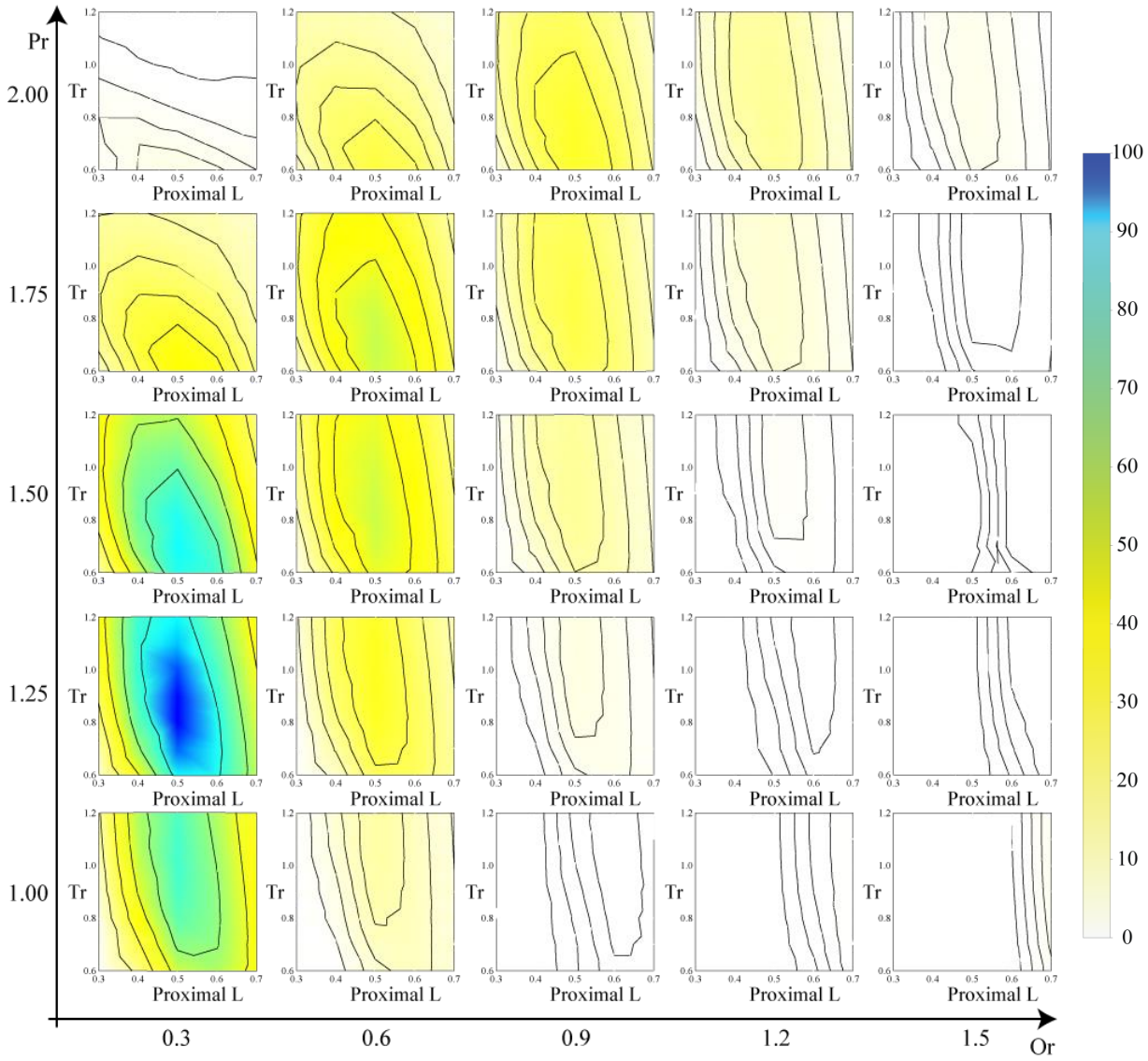

Fig. 10 Evolution of the size of the workspaces for underactuated hands. We show contour plots between transmission ratio and proximal link lengths across different palm and object sizes, with the rest of the parameters fixed to $\alpha = \beta = \pi/3$ and $K_r = 4$.

Table IV Range of values of the parameters for the results in Fig. 10 and 11.

Parameter	Range	Step
P_r	1.5	–
l	(0.4,0.7)	0.05
O_r	0.5	–
α	(0.84,1.25)	$\pi/30$
β	(0.84,1.25)	$\pi/30$
K_r	7	–
T_r	(0.5,1.3), (0.85,1.05)	0.1,0.05

B. On the palm size

From the results in Fig. 7 we stated that the optimal relationship between size of palm and object was $P_r - O_r \approx 1$, that is, the difference between palm and object diameter similar to the length of the fingers. We study this relationship with more detail in Fig. 10, where we can see the evolution of the contour plots between transmittion ratio vs. proximal link length for different sizes of palm and object for the underactuated hand.

Looking at the axes $P_r - O_r$, we can see how the palm size increaseas in accordance to the object size, as we observed before. In addition, the optimal values are consistently obtained around a $DP_r = 1$, that corresponds to the proximal link length of 0.5. The transmission ratio slightly shifts from high values to lower values when the palm grows from small to big.

C. On the symmetry of the palm and the grasp

We performed a second execution adding the parameters α and β to study the effect on the symmetry of the palm. Note that the variation of α changes the symmetry of the palm, while β changes the symmetry of the grasping points.

We have perfomed several executions exploring randomly the space of all the parameters using the ranges in Table I. Our results indicated that the trends observed in the previous executions were mantained when adding these two extra parameters, but we don't show the results for space reasons. Then, we reduced the parameter space following the results obtained in the previous sections. That is, the size of palm and object grow accordingly, and so, we chose a fixed size object, and the corresponding optimal size of palm. Also, we

Table V: Best fully actuated workspaces for $P_r = 1.5$ and $O_r = 0.5$

Prox L	α	β	F-A	T_r	U-A
0.45	1.25	1.24	93908	0.9	33961
0.45	0.84	0.84	94355	0.9	32387
0.4	1.26	1.24	94827	1.	28361
0.4	0.84	0.84	95097	0.95	26558

can fix the value of the stiffness constant. Therefore, for the execution results shown next, we set $P_r = 1.5$, $O_r = 0.5$ and $K_r = 7$.

For the ranges and the step sizes shown in Table IV, we compute the sizes of the manipulation workspace for all possible combinations. This execution computes a total of 175 workspaces for fully-actuated hands, and a total of 2100 workpaces sizes for the underactuated ones (that consider the extra parameter T_r).

The results of the fully-actuated workspace can be seen in Table V and Fig. 11. The table shows the best 2% sizes of fully-actuated hand workspaces, with their corresponding maximum possible underactuated hand workspaces. In the figure, we show the contour plots between α and β for different proximal link lenghts. In this case, it is clear that the best results are obtained at the lower proximal link length and also at the diagonal $\alpha = \beta$, with slightly better results away from the symmetric configuraiton.

Table V shows, similarly as seen in Table III, that the 2% maximu sizes for underactuated workspace sizes correspond to different geometric parameters. Best size for the underactuated hands range from 39,057 to 38,363, obtained with

$$DP_r = 1, \alpha = \pi/3, \beta = \pi/3 \text{ and}$$
$$T_r = 0.95, 0.8, 0.9, 0.85$$

respectively.

The results for the computation of underactuated hand workspace sizes are shown in Fig. 12. It is clear that all of the optimal sizes are obtained in the digonal $\alpha = \beta$, being the best one the central one, corresponding to the symmetric hand. Observe also that the pattern for the relationship betweeen T_r and DP_r is fairly constant in all the plots, indicating that is not affected by the parameters α and β, with biggest size between the values $T_r \in (0.8,1)$ and DP_r around 1.

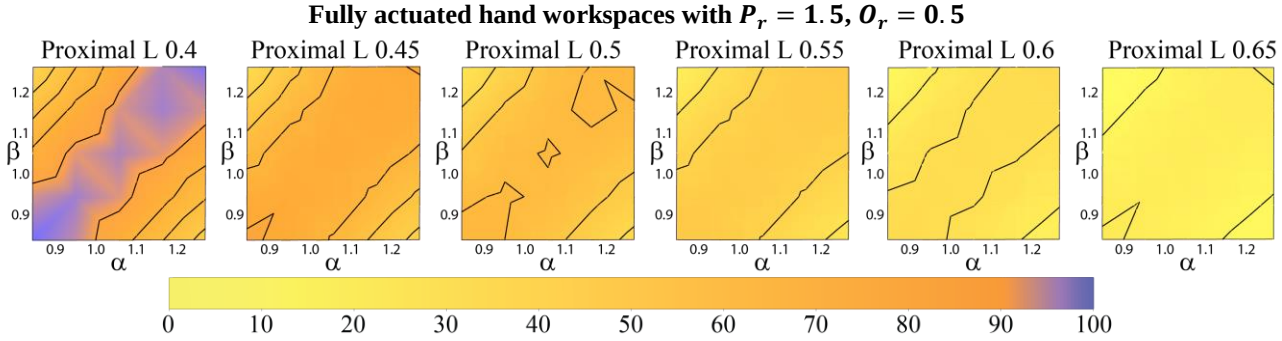

Fig. 11 . Sizes of a fully actuated version of the hand for different proximal link lengths when the symmetry at the palm and at the contact points changes, also for a fix palm and object of $P_r = 1.5$, object to $O_r = 0.5$.

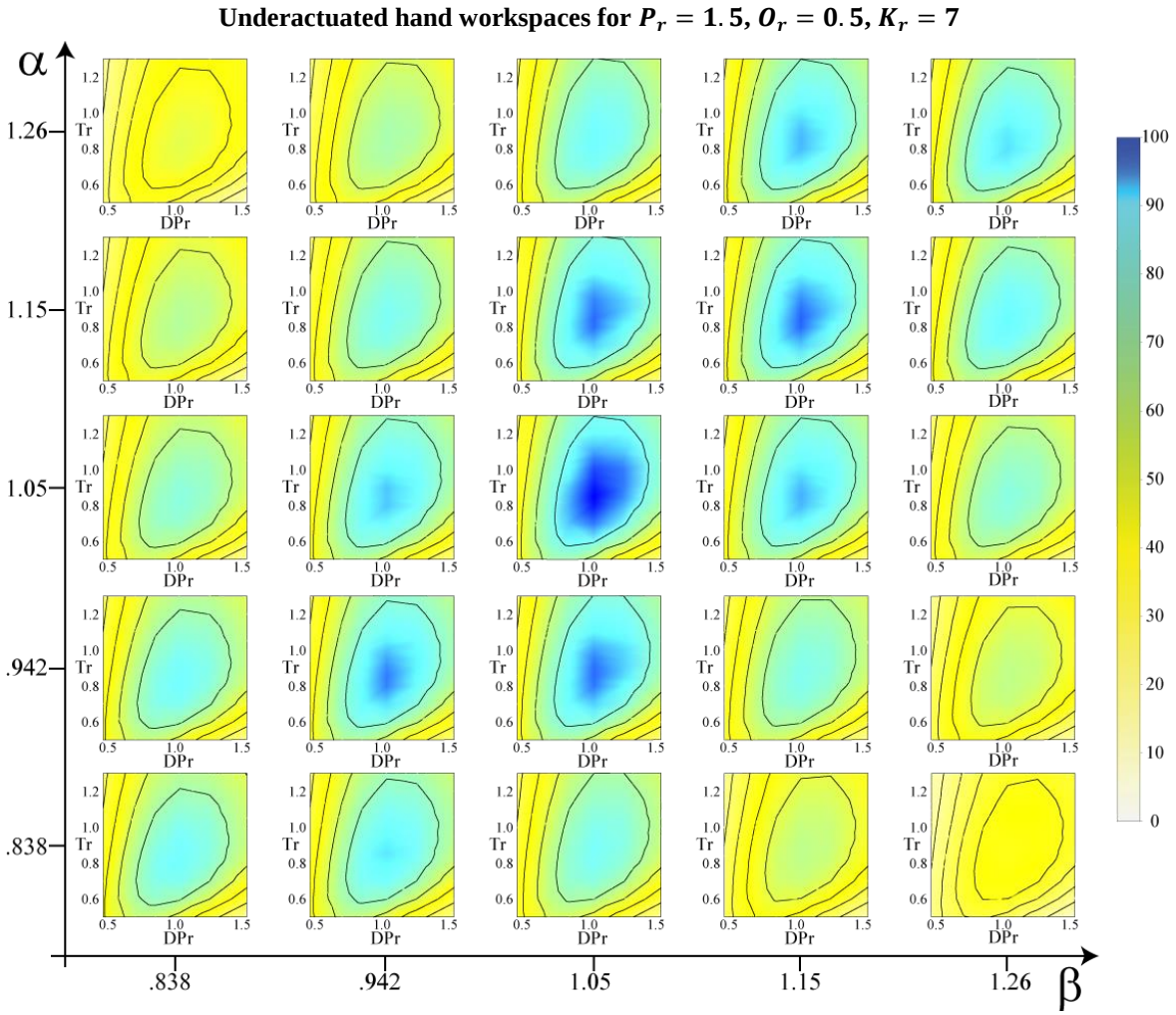

Fig. 12 Graphic of contour plots for different symmetry parameters α and β, for a palm ratio fixed to $P_r = 1.5$, object to $O_r = 0.5$ and $K_r = 7$.

D. Distribution of the Jacobian matrix indexes

To study the quality of the grasp, the grasping literature typically uses different indexes related to the Jacobian matrix of the system. Sometimes this relates only to the Grasp matrix, and sometimes it relates to the combination of both the Grasp matrix and the hand Jacobian (Shimoga, 1996). From our analysis, we want to study how these values look for one hand plus object with optimal workspace size. We have chosen the parameters

$$P_r = 1.5, DP_r = 1, O_r = 0.5, \alpha = \pi/3, \beta = \pi/3,$$
$$K_r = 7, T_r = 0.9,$$

that lead to a fully-actuated hand with 83,566 configurations workspace and a underactuated version with 38,749 (that is a 46.4%).

The most widely used index is the condition number of the matrix $\boldsymbol{J}^T$ (Merlet, 2006b), which is valid for both underactuated and fully actuated hands, and its defined as

$$\kappa(\boldsymbol{J}^T) = \frac{Max[Eigenvalues(\boldsymbol{J}^T\boldsymbol{J})]}{Min[Eigenvalues(\boldsymbol{J}^T\boldsymbol{J})]}.$$

Note that the condition number ranges from 1 to ∞, being 1 the optimal.

However, the matrix that defines the singularities of the static equilibrium equations in the underactauted case is the reduced $\boldsymbol{J}_a$ matrix, that depends on the geometrical parameters and on the transmission ratio T_r. The determinant of $\boldsymbol{J}_a$ gives us an idea of the magnification of the actuation torques for a given external force. For a configuration where its value is close to zero, small external forces may need very big actuation torques to achieve equilibrium. These kind of configurations are called type 2 singularities (Gosselin and Angeles, 1990).

Fig. 13 shows a representation of the position workspace for the fully actuated (black) and the underactuated workspaces (colored) of the same hand. In Fig. 13–(a), each dot color represents the minimum value of $Det(\boldsymbol{J}_a)$ in all the orientations achievable from the dot position. In Fig. 13-(b), each dot color represents the median value of the condition number of $\boldsymbol{J}^T$ in all the orientations achievable from the dot position. The bottom figure shows a piece of the fully-actuated hand workspace, bordering in black the positions that are also inside the underactuated workspace.

We can observe that the determinant of the matrix $\boldsymbol{J}_a$ is bigger than 0.5 in almost all the workspace, being closer to singularity at the border of the workspace. Further analysis is

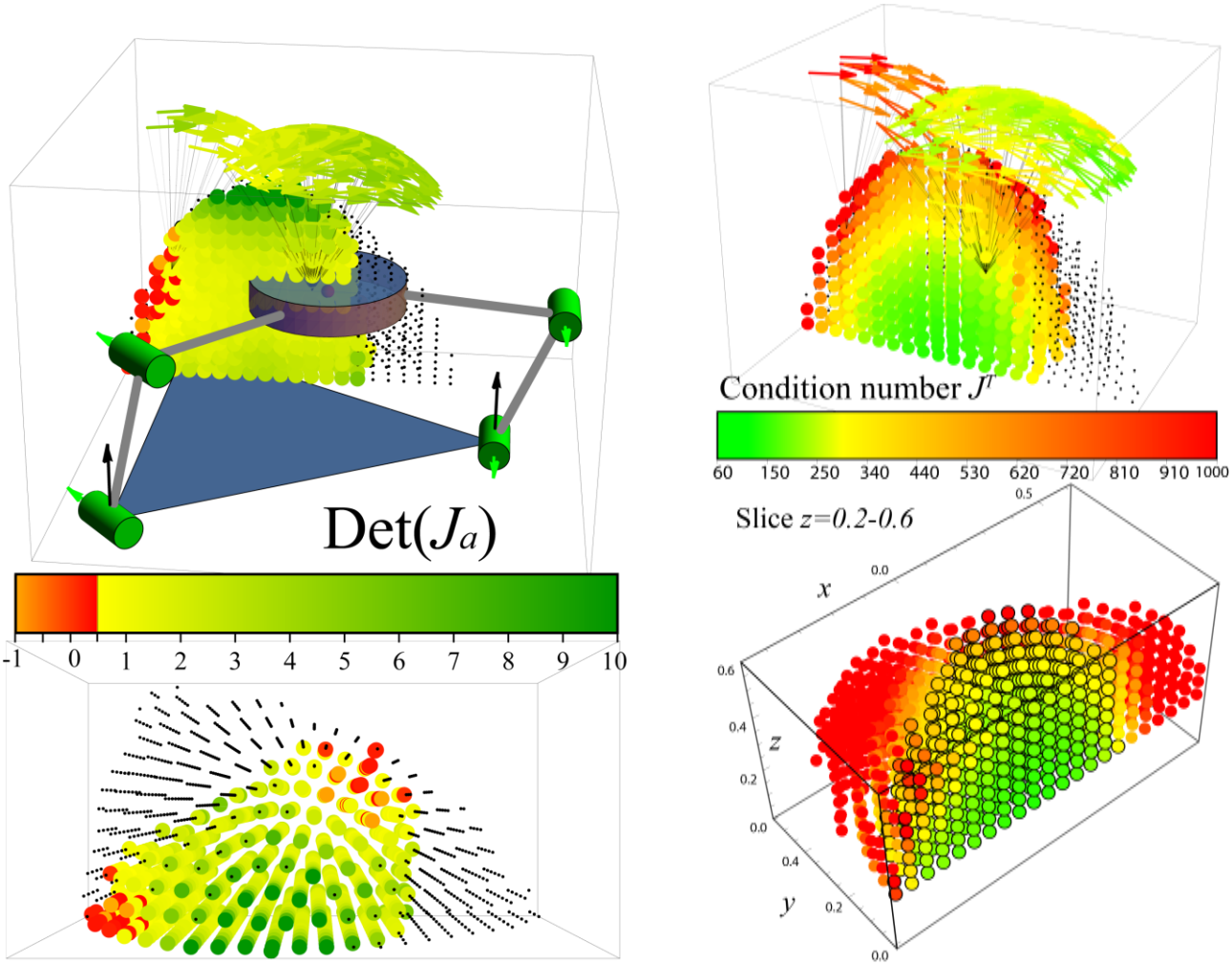

(a) (b)

Fig. 13 Evolution of the determinant of the Jacobian matrix and the condition number for the workspace of a hand with parameters $P_r = 1.5$, $DP_r = 1$, $O_r = 0.5, \alpha = \pi/3, \beta = \pi/3, K_r = 7$, and , $T_r = 0.9$.

needed to know where the second type singularities are located (Gosselin and Angeles, 1990) but preliminary results show that the more optimal workspaces are those where these type of singularities occur outside the reachable workspace.

We can also see in Fig. 13-(b) bottom that the configurations that belong to the underactuated workspace are the ones with lower condition number.

VI. Conclusions

This work uses a framework for robotic hands inspired in the parallel robots literature that computes the manipulation workspace of a hand-plus-object system. This allows us to explore the space of design parameters to find the hand geometry that maximizes the size of the manipulation workspace.

Our computations assume that the normals to the object surface at the contact points are directed towards the center of mass. This covers round shapes including spherical and disk objects, which are the most commonly grasped with the tripod grasp. In addition, we modeled the contact points using the point with friction model, and thus, may not be accurate away from the initial central position $(p_x, p_y) = (0, 0)$. To take that into account, we impose a minimum angle of 120degrees between the normal to the surface of the object at the contact point and the contact phalange.

Without taking into account the limitations on the motors, we have observed that using underactuation can decrease the size of the manipulation workspace significantly up to 80%. However, an optimal choice of the underactuation parameters can lead to an reduction of only 50% of the fully-actuated hand workspace. More importantly, the 50% of the workspace that belongs to the underactuated hand workspace is always located at the center of the object with respect to the hand, which are the most relevant in practice.

Our design parameters exploration has shown several additional interesting results. The diameter of the palm and the diameter of the object are optimal when $P_r - O_r \approx 1$, which means that the radii difference is about half of the length of the finger. Note that for $P_r = O_r$ the fingers are in a singularity at any central configuration $(p_x, p_y) = (0, 0)$, because the fingertip lies in the same (x, y) coordinates that the base of the finger, allowing the rotation of the first joint without modifying the location of the fingertip. Therefore, it makes sense that the optimum is as far away as possible from being in a singular configuration at the center of the workspace, without being as far that disables mobility.

Future work will study if such results are valid when using the antropomorphic adbduction/adduction axis instead of the vertial one in the fingers. However, for all the existing robotic hands using the verital axis, the design of the palm should have a diameter equal to the mean size of object sizes we want to manipulate plus 1, so that they work as well as possible with a wide range of object sizes.

Our results also show that the distal-proximal ratio seems to be optimal when it is close to 1 (for underactauted) or slightly bigger than 1 (for fully-actuated). The ratios that are usually seen in most of 2 link finger hands are smaller than 1, meaning a shorter distal link. This is because dimensional synthesis applied to single fingers shown optimal conditioning at 0.7071 (Salisbury and Craig, 1982), while (Yoshikawa) obtained optimal manipulability and finger workspace volume at a ratio of 1. However, these are results optimizing single fingers, and not the workspace obtained with the combination of all of them. It was expected that our results could indicate slightly different results to optimize manipulation workspace size. Note that if you consider a typical 3 link anthropomorphic finger with the distal joint locked, the ratio between the two distal links and the proximal is closer or even slightly bigger than 1. This indicates that the tripod grasp with antropomorphic three linked fingers is already optimized for workspace size, even if the distal joint is kept fixed.

Our results also show that more optimal workspaces with the tripod grasp are obtained for symmetric placement of the fingers in the hand when the hand is underactuated. Regardless, we have seen that whatever the distribution on the palm, it is best to use the same distribution for the grasp contact points both for the underactuated and for fully-actuated hands. However, this result may be different if we change our assumption on the normal to the object surface pointing towards the center of mass.

We have also shown that, for underactuated hands, increasing the finger stiffness ratio also increases the workspace, at the cost of requiring larger actuation torques.

The optimal transmission ratios were found around 0.9, decreasing slightly for bigger palm sizes independently of the distal-proximal ratio.

The results presented in this paper are valid for the studied three-fingered hand structure using a fully-actuated hand versus an underactuated version of the same hand design. More generally, we can state that the optimal dimensions to obtain big manipulation workspaces are different from others obtained optimizing a single grasp. For instance, for manipulation workspaces, robotic hands seem to need bigger distal-proximal ratios and bigger palms than the ones seen in commercial hands such as the Barret hand or the Schunk SDH hand. Additional analysis would be needed to extend these results to other hand configurations, including allowing the thumb to have a different geometry as well as the analysis of three link fingers as in anthropomorphic configurations.

Optimal design for robotic hands is a challenging problem where many considerations need to be taken into account. A design process involves usually optimization of several criteria. We have shown that manipulation workspace size is a relevant criteria to consider, particularly for underactuated hands, to avoid significant reductions of workspace that can greatly limit the versatility of the final hand design.

VII. Aknowledgement

This work was supported in part by a grant from the National Science Foundation, grant NSF IIS-0953856.

References

Balasubramanian R, Belter JT and Dollar AM. (2012) Disturbance Response of Two-Link Underactuated Serial-Link Chains. *Journal of Mechanisms and Robotics* 4: 021013.

Bicchi A and Prattichizzo D. (2000) Manipulability of Cooperating Robots with Unactuated Joints and Closed-Chain Mechanisms. *IEEE Transactions on Robotics and Automation* 16: 336-345.

Borràs J and Dollar AM. (2013a) Framework comparison between a multifingered hand and a parallel manipulator. *Computational Kinematics*.

Borràs J and Dollar AM. (2013b) A parallel robots framework to study precision grasping and dexterous manipulation. *IEEE Int. Conf. on Robotics and Automation*.

Borràs J and Dollar AM. (2014) Analyzing dexterous hands using a parallel robots framework. *Autonomous Robots* 36: 169-180.

Bullock I, Ma R and Dollar A. (2012a) A Hand-Centric Classification of Human and Robot Dexterous Manipulation. *IEEE Transactions on Haptics* 6: 129 - 144.

Bullock IM, Borràs J and Dollar AM. (2012b) Assessing Assumptions in Kinematic Hand Models: A Review. *IEEE RAS/EMBS International Conference on Biomedical Robotics and Biomechatronics*: 139-146.

Bullock IM, Feix T and Dollar AM. (2013) Finding Small, Versatile Sets of Human Grasps to Span Common Objects. *IEEE International Conference on Robotics and Automation*.

Butterfaß J, Grebenstein M, Liu H and Hirzinger G. (2001) DLR-Hand II: Next generation of a dextrous robot hand. *Robotics and Automation, 2001. Proceedings 2001 ICRA. IEEE International Conference on* 1: 109-114.

Butterfaß J, Hirzinger G, Knoch S and Liu H. (1998) DLR's multisensory articulated hand. I. Hard-and software architecture. *Robotics and Automation, 1998. Proceedings. 1998 IEEE International Conference on* 3: 2081-2086.

Ciocarlie M and Allen P. (2011) A constrained optimization framework for compliant underactuated grasping. *Mech. Sciences* 2: 17-26.

Ciocarlie M, Hicks FM and Stanford S. (2013) Kinetic and Dimensional Optimization for a Tendon-driven Gripper. *IEEE International Conference on Robotics and Automation*: 2751-2758.

Cui L and Dai JS. (2012) Reciprocity-Based Singular Value Decomposition for Inverse Kinematic Analysis of the Metamorphic Multifingered Hand. *Journal of Mechanisms and Robotics* 4: 034502.

Cutkosky MR. (1989) On Grasp Choice, Grasp Models, and the Design of Hands for Manufacturing Tasks. *IEEE Transactions on Robotics and Automation* 5.

Dai JS and Wang D. (2007) Geometric Analysis and Synthesis of the Metamorphic Robotic Hand. *Journal of Mechanical Design* 129: 1191.

Dai JS, Wang D and Cui L. (2009) Orientation and Workspace Analysis of the Multifingered Metamorphic Hand—Metahand. *IEEE Transactions on Robotics* 25: 942-947.

Das I and Dennis JE. (1997) A closer look at drawbacks of minimizing weighted sums of objectives for Pareto set generation in multicriteria optimization problems. *Structural Optimization* 14: 63-69.

Dollar AM and Howe RD. (2010) The Highly Adaptive SDM Hand: Design and Performance Evaluation. *The International Journal of Robotics Research* 29: 585-597.

Gosselin C and Angeles J. (1990) Singularity Analysis of Closed-Loop Kinematic Chains. *IEEE Transactions on Robotics and Automation* 6: 281-290.

Grebenstein M, Albu-Schaffer A, Bahls T, Chalon M, Eiberger O, Friedl W, Gruber R, Haddadin S, Hagn U and Haslinger R. (2011) The DLR hand arm system. *Robotics and Automation (ICRA), 2011 IEEE International Conference on*: 3175-3182.

Grebenstein M, Chalon M, Hirzinger G and Siegwart R. (2010) A Method for Hand Kinematics Designers. 7 Billion Perfect Hands. *International Conference on Applied Bionics and Biomechanics*.

Hammond FL, Weisz J, de la Llera Kurth A, Allen PK and Howe RD. (2012) Towards a design optimization method for reducing the mechanical complexity of underactuated robotic hands. *Robotics and Automation (ICRA), 2012 IEEE International Conference on*: 2843-2850.

Jacobsen S, Iversen E, Knutti D, Johnson R and Biggers K. (1986) Design of the Utah/MIT dextrous hand. *Robotics and Automation. Proceedings. 1986 IEEE International Conference on* 3: 1520-1532.

Kerr J and Roth B. (1986) Analysis of Multifingered Hands. *The International Journal of Robotics Research* 4: 3-17.

Martell JS and Gini G. (2007) Robotic hands: Design review and proposal of new design process. *Proceedings of World Academy of Science, Engineering and Technology* 20: 85-90.

Mason MT and Salisbury JK. (1985) *Robot Hands and the Mechanics of Manipulation*: The MIT Press.

Mason MT, Srinivasa SS and Vazquez AS. (2011) Generality and simple hands. *Robotics Research. Springer Tracts in Advanced Robotics.* Springer, 345-361.

Matsuoka Y, Afshar P and Oh M. (2006) On the design of robotic hands for brain-machine interface. *Neurosurgical focus* 20: 1-9.

Merlet JP. (2006a) Design. *Parallel robots.* Second edition ed.: Springer, 301-320.

Merlet JP. (2006b) Jacobian, Manipulability, Condition Number, and Accuracy of Parallel Robots. *Journal of Mechanical Design* 128: 199-206.

Michelman P. (1998) Precision object manipulation with a multifingered robot hand. *Robotics and Automation, IEEE Transactions on* 14: 105-113.

Mohamed MG and Duffy J. (1985) A Direct Determination of the Instantaneous Kinematics of Fully Parallel Robot Manipulators. *Journal of Mechanisms Transmissions and Automation in Design* 107: 226-229.

Odhner LU and Dollar AM. (2011) Dexterous Manipulation with Underactuated Elastic Hands. *IEEE International Conference on Robotics and Automation*: 5254-5260.

Odhner LU, Jentoft LP, Claffee MR, Corson N, Tenzer Y, Ma RR, Buehler M, Kohout R, Howe RD and Dollar AM. (2013) A compliant, underactuated hand for robust manipulation. *The International Journal of Robotics Research* 33 736-752.

Okada T. (1982) Computer control of multijointed finger system for precise object-handling. *Systems, Man and Cybernetics, IEEE Transactions on* 12: 289-299.

Salisbury JK and Craig JJ. (1982) Articulated Hands: Force Control and Kinematic Issues. *The International Journal of Robotics Research* 1: 4-17.

Schunk. (2013) *SCHUNK Dextrous Hand SDH*. Available at: www.schunk.com.

Shimoga KB. (1996) Robot Grasp Synthesis Algorithms: A Survey. *The International Journal of Robotics Research* 15: 230-266.

Simo-Serra E, Perez-Gracia A, Moon H and Robson N. (2012) Kinematic synthesis of multi-fingered robotic hands for finite and infinitesimal tasks. *Latest Advances in Robot Kinematics.* Springer, 173-180.

Townsend W. (2000) The BarrettHand grasper – programmably flexible part handling and assembly. *Industrial Robot: An International Journal* 27: 181-188.

Tsai L-W. (1999) *Robot Analysis. The mechanics of serial and parallel manipulators*: John Wiley & sons, Inc.

Yoshikawa T. (1985) Manipulability of Robotic Mechanisms. *The International Journal of Robotics Research* 4: 3-9.